

# Thin Film Si-Ge/c-Si Tandem Junction Solar Cells with Optimum Upper Sub- Cell Structure

Jinjoo Park\*

Major of Energy and Applied Chemistry, Division of Energy & Optical Technology Convergence, Cheongju University,  
Cheongju-si 28503, Korea

Received September 9, 2020; Accepted September 14, 2020

**ABSTRACT:** This study was trying to focus on achieving high efficiency of multi junction solar cell with thin film silicon solar cells. The proposed thin film Si-Ge/c-Si tandem junction solar cell concept with a combination of low-cost thin-film silicon solar cell technology and high-efficiency c-Si cells in a monolithically stacked configuration. The tandem junction solar cells using amorphous silicon germanium (a-SiGe:H) as an absorption layer of upper sub-cell were simulated through ASA (Advanced Semiconductor Analysis) simulator for acquiring the optimum structure. Graded Ge composition – effect of  $E_g$  profiling and inserted buffer layer between absorption layer and doped layer showed the improved current density ( $J_{sc}$ ) and conversion efficiency ( $\eta$ ). 13.11% conversion efficiency of the tandem junction solar cell was observed, which is a result of showing the possibility of thin film Si-Ge/c-Si tandem junction solar cell.

**Key words:** 2 terminal tandem junction solar cell, Amorphous silicon germanium, Advanced semiconductor analysis simulator, Conversion efficiency

## 1. Introduction

Solar cell technology depended on efficiency, operational stability and its production cost as three of the most important factors that determined viability of a photovoltaic (PV) technology. The initial efficiency determined the available output power from the device under standard illumination condition, while its characteristic stability profile provided the predicted efficiency in future time scale, and the stability depended on various factors as well. Cost of the module determined acceptability of the device for its large-scale application or use. In the past, a combination of the higher price of the device, lower efficiency and stability made most of the devices not so popular for renewable energy sources. But the things had been changing rapidly and it was foreseeable that more stable, efficient and reduced cost solar cells would be available in future. The progress was taking place in many fronts.

Crystalline Si (c-Si) based solar cells showed a  $J_{sc}$  more than 40 mA/cm<sup>2</sup> but its open circuit voltage ( $V_{oc}$ ) remained low. It might be possible to improve the  $V_{oc}$  by using such a solar cell in a tandem structure with a wide  $E_g$  thin film silicon<sup>1-3)</sup>, compound<sup>4,5)</sup>, organic polymer or perovskite cell<sup>6,7)</sup> at the top.

The advantage of such a cell structure was that the overall performance of the tandem cell improved. That was to make PV modules with higher efficiency than market-leading c-Si while leveraging existing c-Si manufacturing capacity, Si-based tandem approaches had been proposed<sup>1-7)</sup>. Looking into the successful operational principle of two terminal tandem solar cells, spectrum splitting and four terminal tandem cells were also investigated. In the spectrum splitting, the incident radiation was divided into multiple optical beams having desired bands of wavelength. These beams were then incident on specific solar cells that were optimized for those optical bands<sup>8-10)</sup>. Recently four terminal Si based tandem solar cells with a top perovskite sub-cell were investigated that shows a 24.6% efficiency<sup>11)</sup>.

In this paper, the results of research on multi-junction solar cells with thin film a-SiGe:H solar cells and c-Si solar cell tandem junctions were studied.

## 2. Experimental

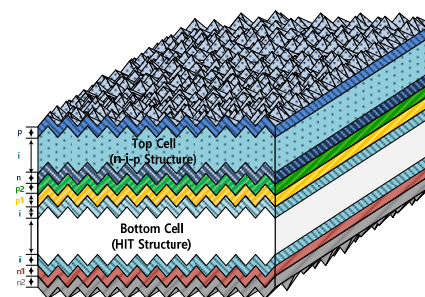
A commercial Czochralski-grown n-type wafer (resistivity of 2.7  $\Omega \cdot \text{cm}$ , thickness of 200  $\mu\text{m}$ ) was used as an absorber material for the bottom cell on Si based multi junction solar cell. The typical sequence was pre-texture cleaning texturization and

\*Corresponding author: [jwjh3516@cju.ac.kr](mailto:jwjh3516@cju.ac.kr)

**Table 1.** Deposition conditions of thin film Si-Ge/c-Si tandem junction solar cells

Layer	Temp. (°C)	Power (W)	Gap (mm)	Press. (mTorr)	Gas flow (sccm)						Thickness (nm)
					SiH <sub>4</sub>	H <sub>2</sub>	GeH <sub>4</sub>	CO <sub>2</sub>	PH <sub>3</sub>	B <sub>2</sub> H <sub>6</sub>	
Bottom cell	i	200	50	20	1500	60	480				5
	n <sub>1</sub>	200	130	20	3000	33	3000		18.3		20
	n <sub>2</sub>	200	280	20	3000	33	1000		6.7		140
	i	200	50	20	1500	60	480				5
	p <sub>1</sub>	200	250	12	5000	30	2700			6.4	5
	p <sub>2</sub>	200	250	12	5000	40	1600			33.3	3
Buffer	p-type nc-Si:H	180	300	20	1500	5	800			0.3	75
Top cell	n	180	50	40	200	30	120		30		40
	n/i buffer (With or without)	180	20	20	400	10	40				10
	I (With or without)	180	25	25	300	5	20	5			200
	I (With or without)	180	25	25	300	5	20	7			200
	i	180	25	25	300	5	20	9			200
	i/p buffer (With or without)	180	20	20	400	10	40				20
	p <sub>1</sub>	180	20	20	1500	5	500		10	1.5	10
	p <sub>2</sub>	180	300	20	1500	5	800			0.3	25

post-texture cleaning. In pre-texture cleaning step, acetone dipping, SC1 (NH<sub>4</sub>OH:H<sub>2</sub>O<sub>2</sub>:Deionized Water (DIW) = 1:1:6) were done and standard texturing process by KOH was conducted for 25 minutes. To remove organic residues from silicon wafers, the famous SC1 and SC2 (HCl:DIW = 1:10) cleaning process were performed after ultrasonic treatment. A chemical polishing (CP) with HNO<sub>3</sub>:CH<sub>3</sub>COOH:HF=15:10:1 was done. Right before a-Si:H layer deposition, the wafers was dipped into 1% hydrofluoric acid for a few minutes. Seconds dipping in HF 3 wt% for 90 s was carried out in order to remove the native oxide before loading to PECVD chamber. The a-Si:H (p/i/n) layers were deposited on the silicon wafer by plasma-enhanced chemical vapor deposition (PECVD) with radio frequency (RF) of 13.56 MHz. At the front side of the wafers, the a-Si:H (i) passivation layer and a-Si:H (p) emitter layer were deposited, first. Then, the a-Si:H (i) and a-Si:H (n+) layers were deposited at the back side. The deposition conditions of the a-Si:H (i/n+) were kept unchanged, while the gas phase doping ratio and hydrogen dilution ration of the emitter bi-layer (a-Si:H (p/p+)) were altered to enhance the quality of the emitter. After that the cell was dipped into 1% hydrofluoric acid for 60 seconds in order to remove the native oxide for improve the interface properties. The p-type nc-Si:H layer was deposited forming a tunnel junction layer with n-type layer of top cell. The n-type a-Si:H, n/i buffer, i-type SiGe:H, i/p buffer p-type a-SiOx:H and p-type nc-Si:H layers were deposited in that order. Detailed deposition conditions for the Si based tandem junction solar cell

**Fig. 1.** Schematic diagram of Si-based tandem junction solar cell

could be referred to Table 1. Indium tin oxide thin film with 200±5 nm thickness was then deposited by radio frequency magnetron sputtering with 6 mm×6 mm shadow mask, followed by evaporation of aluminum as fingers for the front electrodes and silver on the entire rear surface for back contact. The area of the solar cells was 0.36 cm<sup>2</sup>. A schematic diagram of the 2 terminals tandem junction solar cell is shown in Fig. 1.

### 3. Results and discussion

#### 3.1 Properties of 2 terminal Si-based tandem junction solar cells with different absorption layer of top cell

$J_{sc}$  of c-Si based solar cell was about 40 mA/cm<sup>2</sup> and the  $J_{sc}$  of series connected tandem junction solar cells was matched by low in either of sub-cells. The matched  $J_{sc}$  on the series connected Si-based tandem junction solar cell was main factor

**Table 2.** Classification of the 2 terminal Si-based tandem junction solar cells depending on the absorption material of top sub-cell and briefly results by ASA simulation

2 Terminal tandem junction solar cell			
No.	Classification	Top (i)	Bottom
1	Materials	a-Si:H ( $E_g$ :1.81 eV)	c-Si (1.1 eV)
2		a-SiGe:H ( $E_g$ :1.65 eV)	
3		a-SiGe:H ( $E_g$ :1.45 eV)	
4		$\mu$ c-Si:H ( $E_g$ :1.1 eV)	

for obtain high efficiency. The getting higher  $J_{sc}$  on 2 terminal Si-based tandem junction solar cells means obtaining higher efficiency which is related with the improved  $J_{sc}$  of top sub-cell. The  $J_{sc}$  of the cells was mainly associated with the  $E_g$  of absorption materials, structure, quality and surface morphology.

First of all, the properties of the 2 terminal Si-based tandem junction solar cells with different absorption layer of the top sub-cell was investigated by ASA simulation. There were 4 kinds of the absorption materials for top sub-cell such as a-Si:H ( $E_g$ :1.81 eV), a-SiGe:H ( $E_g$ :1.65 eV or 1.45 eV) and  $\mu$ c-Si:H ( $E_g$ :1.1 eV) was considered. Fig. 1 showed the schematic structure of the 2 terminal Si-based tandem junction solar cells. The optimum structure and thickness (p-nc-Si:H/ p-a-SiOx:H/ i-layer/ n-a-Si:H/ p-nc-Si:H/ Si/ n-nc-Si:H) was used for analysis of the 2 terminal Si-based tandem junction solar cells. Table 2 showed the classifications of 2 terminal Si-based tandem junction solar cells and the brief results depending on absorption material of top sub-cell. The Si (1.1 eV) was surely fixed for the bottom sub-cell. That was assigned no.1 was a-Si:H (1.81 eV), no.2 was a-SiGe:H (1.65 eV), no.3 was a-SiGe:H (1.45 eV) and no.4 was  $\mu$ c-Si:H (1.1 eV) of top sub-cell, individually. The  $J_{sc}$  and the  $V_{oc}$  was commonly the trade-off relation. The case of the no.4, the material with the lowest  $E_g$  of top sub-cell among the cases, presented the highest  $J_{sc}$  and the lowest  $V_{oc}$ . In contrast the no.1 was the highest  $E_g$  indicated the lowest  $J_{sc}$  and the highest  $V_{oc}$ . The important thing was the valence of  $J_{sc}$  and  $V_{oc}$  and other thing was FF by maintain a high value. That explanation was indicated in Table 3. The suitable material was a-SiGe:H for applying of absorption layer of top sub-cell to 2 terminal Si-based tandem junction solar cells. Table 3 expressed solar cell parameters of 2 terminal Si-based tandem junction solar cells. The no.1 showed the lowest  $J_{sc}$  of 16.06 mA/cm<sup>2</sup>, the highest  $V_{oc}$  of 1.657 V, an FF of 79.66%,

**Table 3.** Solar cell device parameters of 2 terminal Si-based tandem junction solar cells by ASA simulation

No.	$J_{sc}$ (mA/cm <sup>2</sup> )	$V_{oc}$ (V)	FF (%)	$\eta$ (%)
1	16.06	1.657	79.66	21.19
2	20.63	1.486	78.72	24.14
3	22.83	1.340	70.22	21.47
4	25.22	1.235	69.24	21.56

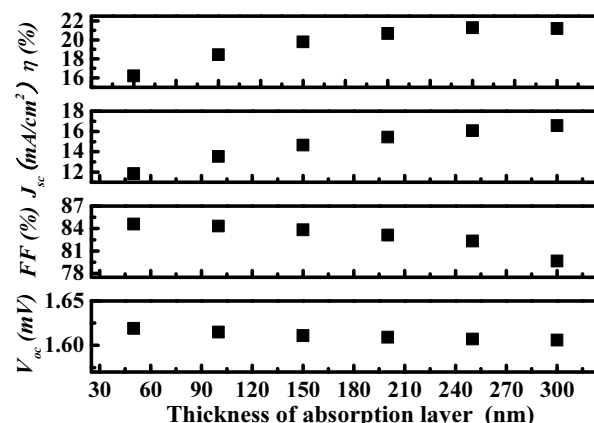


**Fig. 2.** The optimized thickness of the a-Si:H (1.81 eV) for top sub-cell on 2 terminal c-Si-based tandem junction solar cells by ASA simulation

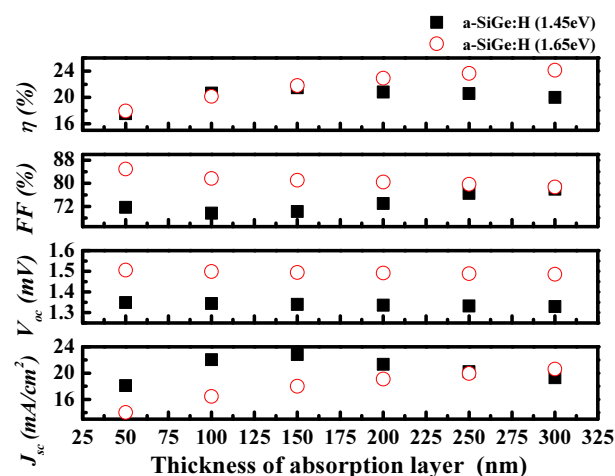


**Fig. 3.** The optimized thickness of the a-SiGe:H (1.65 eV and 1.45 eV) for top sub-cell on 2 terminal Si-based tandem junction solar cells by ASA simulation

and  $\eta$  of 21.19%. The no.2 showed the  $J_{sc}$  of 20.63 mA/cm<sup>2</sup>, the  $V_{oc}$  of 1.486 V, an FF of 78.72%, and the highest  $\eta$  of 24.14%. The no.3 showed the  $J_{sc}$  of 22.83 mA/cm<sup>2</sup>, the  $V_{oc}$  of 1.34 V, an FF of 70.22%, and  $\eta$  of 21.47%. The no.4 showed the highest  $J_{sc}$  of 25.22 mA/cm<sup>2</sup>, the lowest  $V_{oc}$  of 1.23 V, an FF of 69.24%, and  $\eta$  of 21.56%. In addition to Figs. 2 and 3 showed optimized thickness of the absorption materials (except no.4- the results depending on thickness were meaningless) for top sub-cell on 2 terminal Si-based tandem junction solar cells by ASA

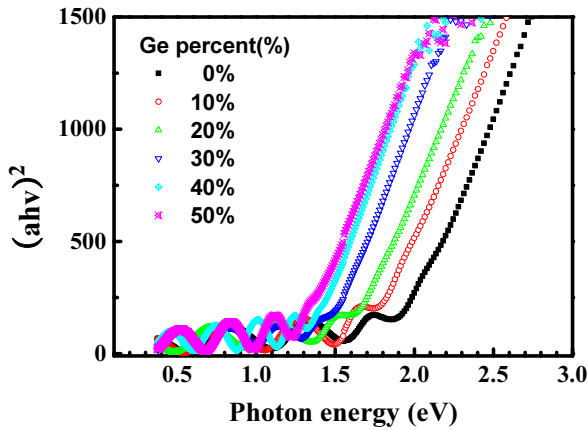


Fig. 4. Tauc's plot of a-SiGe:H depending on Ge ratio

simulation. With increased thickness of absorption layer of solar cells, the  $J_{sc}$  was increased and the FF was dropped. Fig. 2 indicated a-Si:H (1.81 eV) of the 300 nm thick for top sub-cell was appropriated which showed a  $J_{sc}$  of 16.06 mA/cm<sup>2</sup>, a  $V_{oc}$  of 1.657 V, an FF of 79.66%, and  $\eta$  of 21.19%.

Fig. 3 explained a-SiGe:H (1.65 eV) of the 300 nm thick for top sub-cell was appropriated which showed the  $J_{sc}$  of 20.63 mA/cm<sup>2</sup>, the  $V_{oc}$  of 1.48 V, an FF of 78.72%, and  $\eta$  of 24.14%. And Fig. 3 explained a-SiGe:H (1.45 eV) of the 150 nm thick for top sub-cell was appropriated which showed the  $J_{sc}$  of 22.83 mA/cm<sup>2</sup>, the  $V_{oc}$  of 1.34 V, an FF of 70.22%, and  $\eta$  of 21.47%.

### 3.2 Optimization of Si-Ge absorption layer of top cell for applying 2 terminal tandem junction solar cells

#### 3.2.1 Optical bandgap engineering depending on germanium ratio

The carriers were generated in the intrinsic (i) layer of amorphous silicon thin film solar cells and it affected the electrical and optical properties. The property of i-layer was related to the  $J_{sc}$  and FF. The a-SiGe:H was used as the i-layer. The dependence of bandgap on the germanium (Ge) gas ratio was studied. Figs. 4 and 5 showed that as the Ge gas injection ratio increased from 0% to 50%, the optical band gap dropped from 1.84 V to 1.24 V.

The quantum efficiency of actually fabricated amorphous silicon germanium thin film solar cell was shown in Fig. 6. It could be seen that the optical band gap decreased as the Ge gas ratio was increased and the peak shifts from 520 nm to 590 nm increasing the generation of carriers above 900 nm wavelength.

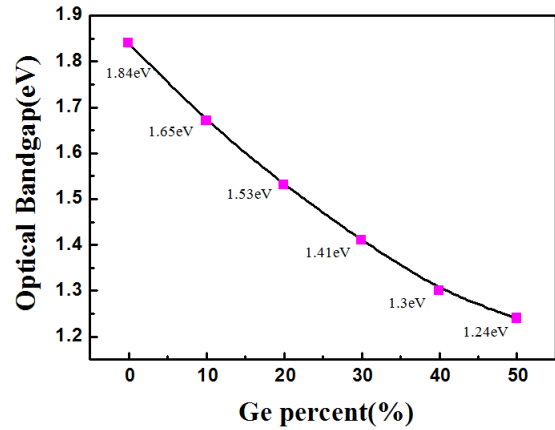
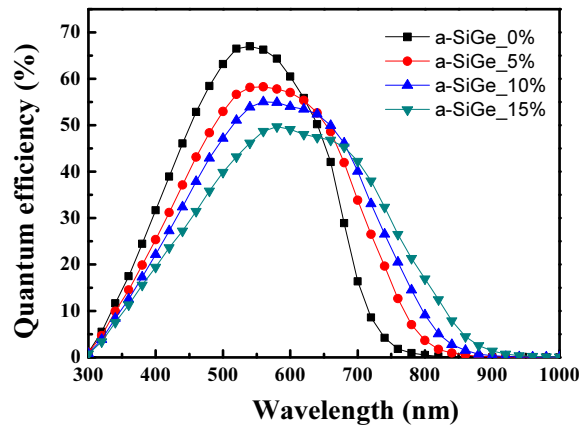
Fig. 5.  $E_g$  of a-SiGe:H depending on Ge ratio

Fig. 6. Quantum efficiency of thin film a-Si solar cells with different Ge ratio in a-SiGe:H absorber layer

Table 4. Conditions of thin film silicon solar cell for optimizing results

Layer	Thickness (nm)	$E_a$ (eV)	$E_g$ (eV)
TCO (FTO)	800	-	-
p-a-Si:H (0.05%)	5	0.51	1.81
p-a-SiOx:H (0.25%)	10	0.53	2.05
p/i buffer	10	-	Variable
i-a-SiGe (10%)	200	-	1.65
i/n buffer	10	-	Variable
n-a-Si:H (1%)	25	0.2	1.81

#### 3.2.2 Optimization of graded buffer (n/i and i/p) layer

##### 3.2.2.1 Optimization of $E_g$ for n/i and i/p buffer layer

The drawbacks of reported a-SiGe solar cells were low FF and  $V_{oc}$ <sup>12)</sup> Using ASA simulator, the FF and  $V_{oc}$  were improved by optimizing n/i and i/p buffer layers. First, optimum band gap of n/i and i/p buffer layers were simulated. The simulation conditions of optimizing the buffer layers were listed in Table 4. Fig. 7 showed the structure for the simulation. The thickness of buffer layer is fixed at 10 nm and the band gap was varied from

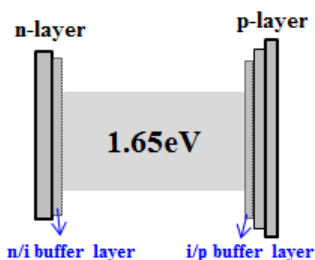


Fig. 7. Band diagram of thin film silicon solar cell with n/i and i/p buffer layers

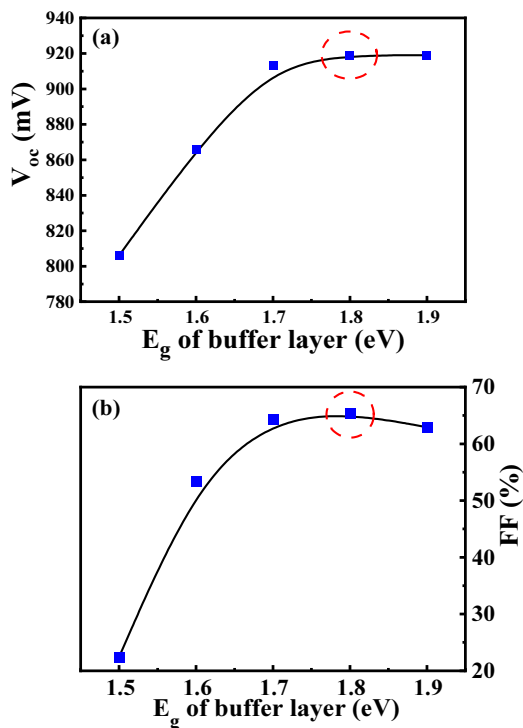


Fig. 8. (a) The  $V_{oc}$ , and (b) FF parameters of thin film silicon solar cell with different  $E_g$  of n/i and p/i buffer layers

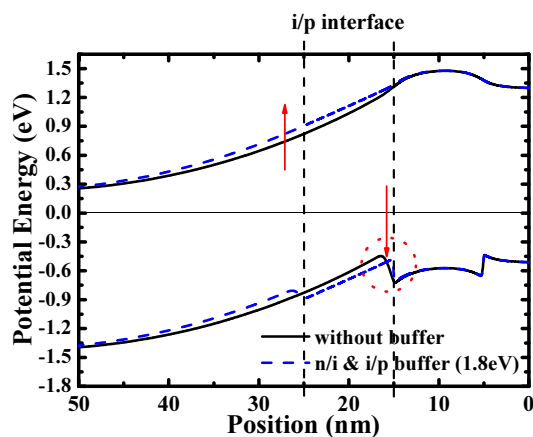


Fig. 9. Band diagrams of thin film solar cells with and without n/i and i/p buffer layers

1.5 eV to 1.9 eV. Fig. 8 showed that FF and  $V_{oc}$  are better than those without buffer layers when the band gap was more than

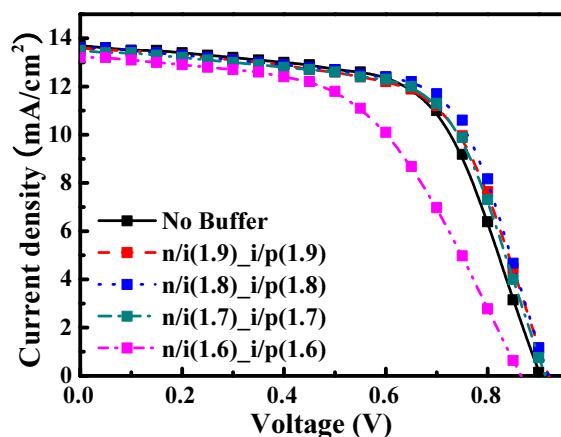


Fig. 10. I-V curves of solar cells with and without n/i and i/p buffer layer ( $E_g$  variation) obtained by ASA simulator

Table 5. Photovoltaic parameters of thin film silicon solar cells with n/i and i/p buffer layers with different  $E_g$

SET	$V_{oc}$ (mV)	$J_{sc}$ (mA/cm <sup>2</sup> )	FF (%)	Eff. (%)
No buffer	902	13.7	62.90	7.78
n/i (1.9)_i/p (1.9)	919	13.6	62.94	7.88
n/i (1.8)_i/p (1.8)	919	13.6	65.42	8.20
n/i (1.7)_i/p (1.7)	919	13.5	64.33	7.95
n/i (1.6)_i/p (1.6)	866	13.2	53.37	6.12
n/i (1.5)_i/p (1.5)	806	9.43	22.42	1.70

1.68 eV but they decrease noticeably when the band gap was lower than 1.68 eV. This could be explained by the band diagram of Fig. 9. When buffer layers were used, the potential barrier of holes at the valence band i/p interface decreased and the conduction band was raised increasing the FF and  $V_{oc}$ . Fig. 10 showed I-V properties of solar cells with and without n/i and i/p buffer layer ( $E_g$  variation) obtained by ASA simulator. Table 5 showed that the optimum band gap of n/i and i/p buffer layers is 1.8 eV.

### 3.2.2.2 Optimization of thickness for n/i and i/p buffer layer

The optimum bandgap was found to be 1.8 eV when the thickness of n/i and i/p buffer layers was 10 nm. These cases, the band gap was fixed at 1.8 eV and the thickness was varied from 4 nm to 12 nm.

The band diagram in Fig. 11 showed that as it got thicker, potential barrier of holes at valence band was decreased and the conduction band was slightly increased resulting in increased FF and  $V_{oc}$ . Table 6 presents parameters of thin film solar cells with n/i and i/p buffer layer with different thickness of the buffer layer. It could be concluded that the best solar cell efficiency was obtained when the thickness of buffer layers

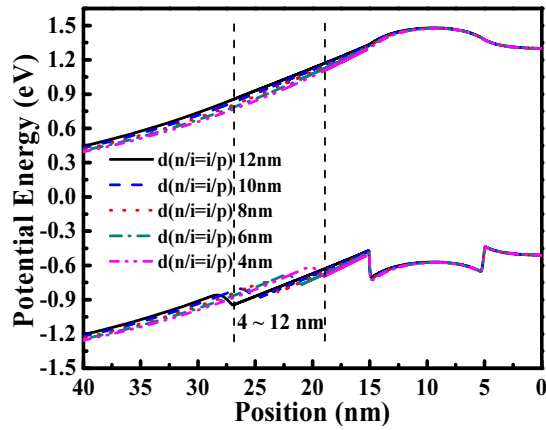


**Fig. 11.** Band diagrams of thin film solar cells with different thickness of n/i and i/p buffer layer

**Table 6.** Photovoltaic parameters of thin film silicon solar cells with n/i and i/p buffer layers with different buffer layer thickness

SET	$V_{oc}$ (mV)	$J_{sc}$ (mA/cm <sup>2</sup> )	FF (%)	Eff. (%)
n/i (1.8)_i/p (1.8)_12_12 nm	921	13.6	65.85	8.24
n/i (1.8)_i/p (1.8)_10_10 nm	919	13.6	65.42	8.20
n/i (1.8)_i/p (1.8)_8_8 nm	915	13.7	64.87	8.13
n/i (1.8)_i/p (1.8)_6_6 nm	912	13.7	64.54	8.08
n/i (1.8)_i/p (1.8)_4_4 nm	909	13.8	64.33	8.05

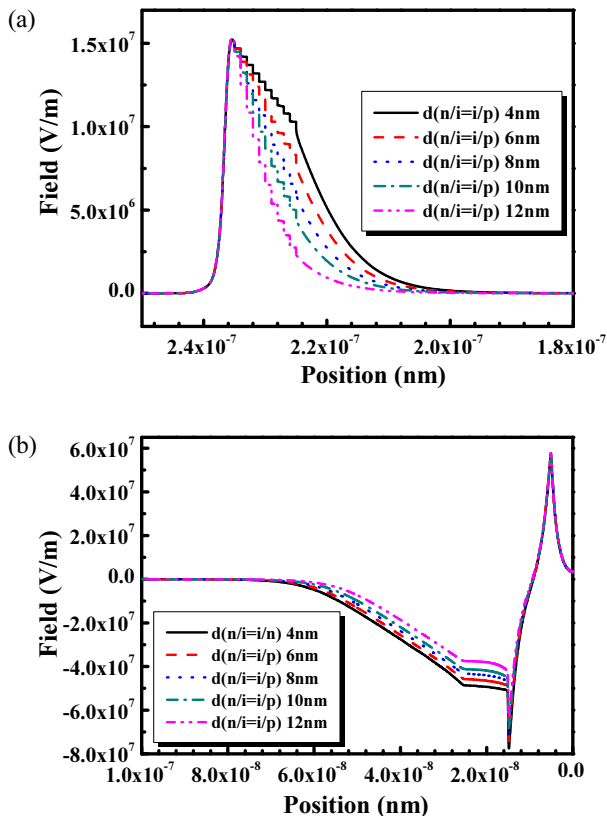


**Fig. 12.** Electric fields at (a) n/i or (b) i/p interface on thin film SiGe solar cell

was 10-12 nm. Fig. 12 showed the as the thickness of buffer layer gets thinner than 10 nm, the field got stronger and the collection of carriers increased resulting in increased  $J_{sc}$ .

### 3.3 Fabrication of 2 terminals thin film Si-Ge/c-Si tandem junction solar cells

The 2 terminals c-Si based tandem junction solar cells were fabricated based on the optimized simulation results (3.1 and 3.2) of the 2 terminals c-Si-based tandem junction solar cells and the thin film a-SiGe:H grading structure for top sub-cell. The I-V characteristics curve and external quantum efficiency of the 2 terminal Si based tandem junction solar cells with different type of absorption layer showed in Fig. 13 and Table 7.

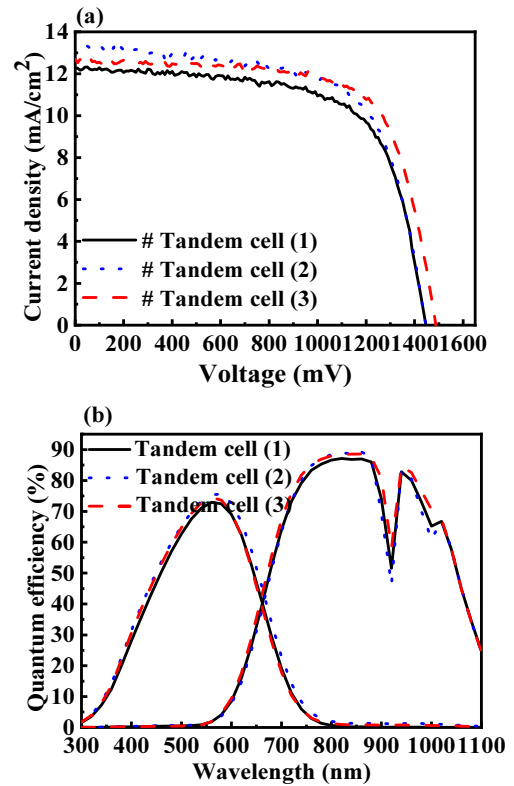


**Fig. 13.** (a) I-V characteristics curve measured at room temperature under AM 1.5 G condition, and (b) external quantum efficiency of the 2 terminal Si based tandem junction solar cells with different type of absorption layer

**Table 7.** Solar cell parameters calculated by I-V characteristics curve of 2 terminal Si based tandem junction solar cell with different absorption layer

No.	$V_{oc}$ (V)	$J_{sc}$ (mA/cm <sup>2</sup> )	FF (%)	Eff. (%)
1	1.44	12.26	67.01	11.84
2	1.44	13.26	66.07	12.62
3	1.48	12.53	70.71	13.11

A 75 nm thick p-type nc-Si:H inter layer used for tunneling junction layer on all 2 terminal Si based tandem junction solar cells based on previously results<sup>13)</sup>. At first variation of the absorption layer for top sub-cell was carried out with the fixed other layers. a a-SiGe:H with 1.55 eV of  $E_g$  applied to absorption layer of top sub-cell for the higher  $J_{sc}$ . The drawbacks of reported a-SiGe:H were low FF and  $V_{oc}$ . For the high  $\eta$ , the optimization of the buffer layer such as n/i and i/p and the bandgap configuration of absorption layer for the top a-SiGe:H sub-cells were needed. Concentrate, type 1) 600 nm thick Si-Ge with 1.55 eV of  $E_g$  - type of the constant Ge concentration, type 2) 600 nm thick a-SiGe:H with a 10 nm thick a-Si:H (1.8 eV of  $E_g$ ) at n/i and i/p interface, type 3) 200 nm thick a-SiGe:H with 1.65 eV of  $E_g$ /200 nm thick a-SiGe:H with 1.60 eV of  $E_g$ /200 nm thick a-SiGe:H with 1.55 eV of  $E_g$  - gradually increased profile of Ge composition in the direction of the n-type layer were tried to fabricate on the absorption layer of top sub-cell. Type 1 displayed a  $V_{oc}$  of 1.44 V, a  $J_{sc}$  of 12.26 mA/cm<sup>2</sup>, an FF of 67.01%, and an  $\eta$  of 11.84%. When the n/i and i/p buffer layers were used, the potential barrier of holes at the valence band i/p interface decreases and the conduction band was raised increasing the FF and  $V_{oc}$  in theoretically. However, the type 2 was not changed on the  $V_{oc}$  and FF. The improved  $J_{sc}$  and spectral response results in Fig. 13 showed that might be buffer layers did not work for reliving discontinued band which played a role in reduced high defect density at the n/i and i/p interfaces<sup>14,15)</sup> and then lessened recombination of carriers<sup>16,17)</sup>. The type 3 was absorption a-SiGe:H layer with gradually increased profile of Ge composition in the direction of the n-type layer. Type 3 was found that the best FF and  $V_{oc}$  was obtained with the thickness of increasing band gap in a-SiGe:H layer and i/p buffer layer was inserted in this structure to increase  $J_{sc}$ . The movement of carriers might get easier improving FF and  $V_{oc}$  in graded a-SiGe:H layer. As a result,  $V_{oc}$  of 1.48 V,  $J_{sc}$  of 12.53 mA/cm<sup>2</sup>, FF of 70.71% and efficiency of 13.11% were obtained which was very promising. The present approach to optimize the bandgap profile by grading Ge composition was thus expected to be very useful to obtain highly efficient 2 terminal thin film Si-Ge/c-Si tandem junction solar cells.

## 4. Conclusions

For high efficiency of 2 terminals c-Si based tandem junction solar cells, structures of top cell were optimized. First, the

optimal structural results were obtained with the ASA simulator. As a result, it was possible to secure a higher current density and FF when the band gap became narrower and the buffer layer was inserted at the interface before and after the a-SiGe:H absorption layer. The role of the buffer layer was attributed to significantly diminish the band-offset between high band gap p-layer and narrow-gap intrinsic a-SiGe:H layer. With optimized top cell structure, the thin film SiGe/c-Si tandem junction solar cells are supposed to further improve the  $V_{oc}$ , 1.48 V and as a result the performance, 13.11% of the 2 terminals tandem junction configuration solar cells.

## Acknowledgments

This works was supported by the research grant of Cheongju University (2019.03.01.~2021.02.28.).

## References

1. Loper, P., Niesen, B., Moon, S.J., De Nicolas, S.M., Holovsky, J., Remes, Z., Ledinsky, M., Haug, F.J., Yum, J.H., De Wolf, S., Ballif, C., "Organic-inorganic halide perovskites: Perspectives for silicon-based tandem solar cells," *IEEE J. Photovoltaics*, Vol. 4, No. 6, pp. 1545-1551, 2014.
2. Sameshima, T., Takenezawa, J., Hasumi, M., Koida, T., Kaneko, T., Karasawa, M., Kondo, M., "Multi junction solar cells stacked with transparent and conductive adhesive," *Jpn. J. Appl. Phys.*, Vol. 50, No. 5R, 052301, 2011.
3. Janz, S., Schnabel, M., LÖper, P., Summonte, C., Canino, M., LÓpez-Vidrier, J., Hernández, S., Garrido, B., Glunz, W.W., "Processing and characterisation of tandem solar cells from crystalline silicon materials," 28<sup>th</sup> European PV Solar Energy Conference and Exhibition, Paris, France, 2013.
4. Umeno, M., Soga, T., Baskar, K., Jimbo, T., "Hetero epitaxial technologies on Si for high-efficiency solar cells," *Sol. Energy Mater. Sol. Cells*, Vol. 50, No. 1-4, pp. 203-212, 1998.
5. Tanabe, K., Watanabe, K., Arakawa, Y., "III-V/Si hybrid photonic devices by direct fusion bonding," *Nat. Sci. Rep.*, Vol. 2, 349, 2012.
6. Bailey, Z.M., McGehee, M.D., "Modeling low cost hybrid tandem photovoltaics with the potential for efficiencies exceeding 20%," *Energy Environ. Sci.*, Vol. 5, pp. 9173-9179, 2012.
7. Bailie, C.D., Christoforo, M.G., Mailoa, J.P., Bowering, A.R., Unger, E.L., Nguyen, W.H., Burschka, J., Pellet, N., Lee, J.Z., Grätzel, M., Noufi, R., Buonassisi, T., Salleo, A., McGehee, M.D., "Semi-transparent perovskite solar cells for tandems with silicon and CIGS," *Energy Environ. Sci.*, Vol. 8, pp. 956-963, 2015.
8. Blocker, W., "High-efficiency solar energy conversion through



- flux concentration and spectrum splitting," *Proc. IEEE*, Vol. 66 pp. 104-105, 1978.
9. Kim, S., Kasashima, S., Sichanugrist, P., Kobayashi, T., Nakada, T., Konagai, M., "Development of thin-film solar cells using solar spectrum splitting technique," *Sol. Energy Mater. Sol. Cells*, Vol. 119, pp. 214-218, 2013.
  10. Wang, X., Waite, N., Murcia, P., Emery, K., Steiner, M., Kiamilev, F., Goossen, K., Honsberg, C., Barnett, A., "Lateral spectrum splitting concentrator photovoltaics: direct measurement of component and submodule efficiency," *Prog. Photovoltaics Res. Appl.*, Vol. 20, pp. 149-165, 2012.
  11. Yan, J., Thomas, F., Romain, C., Galo, T. S., Thierry, M., Stefano, P., Rolf, E., Marta, D.R., Mario, O., Ramis, H., Ayodhya, N.T., and Fan, F., "High-mobility  $\text{In}_2\text{O}_3$ :H electrodes for four-terminal perovskite/ $\text{CuInSe}_2$  tandem solar cells," *ACS Nano*, Vol. 14, No. 6, pp. 7502-7512, 2020.
  12. Lundszen, D., Finger, F., and Wagner, H., "A-Si:H buffer in a-SiGe:H solar cells," *Solar Energy Materials & Solar Cells*, Vol. 74, pp. 365-372, 2002.
  13. Park, J., Kim, S., Phong, P. D., Lee, S., Yi, J., "Improved carrier tunneling and recombination in tandem solar cell with p-type nanocrystalline Si intermediate layer," *Current Photovoltaic Research*, Vol. 8, No. 1, pp. 6-11, 2020.
  14. Lundszen, D., Finger, F., Wagner, H., "Band-gap profiling in amorphous silicon-germanium solar cells," *Appl. Phys. Lett.*, Vol. 80, 1655, 2002.
  15. Arya, R.R., Catalano, A., Oswald, R.S., "Amorphous silicon p-i-n solar cells with graded interface," *Appl. Phys. Lett.*, Vol. 49, 1089, 1986.
  16. Zimmer, J., Stiebig, H., Wagner, H., "a-SiGe:H based solar cells with graded absorption layer," *J. Appl. Phys.*, Vol. 84, 611, 1998.
  17. Fan, Q. H., Chen, C., Liao, X., Xiang, X., Zhang, S., Ingler, W., Adiga, N., Hub, Z., Cao, X., Du, W., Deng, X., "High efficiency silicon-germanium thin film solar cells using graded absorber layer," *Sol. Energy Mater. Sol. Cells*, Vol. 94, 1300, 2010.